

## Article

# The Effect of Lysozyme on the Aggregation and Charging of Oxidized Carbon Nanohorn (CNHox) in Aqueous Solution

Zhengjian Tian <sup>1</sup>, Maolin Li <sup>1</sup>, Takuya Sugimoto <sup>2</sup>  and Motoyoshi Kobayashi <sup>2,\*</sup> 

<sup>1</sup> Graduate School of Science and Technology, University of Tsukuba, 1-1-1 Tennodai, Tsukuba 305-8572, Ibaraki, Japan; s2330328@u.tsukuba.ac.jp (Z.T.); s2130299@u.tsukuba.ac.jp (M.L.)

<sup>2</sup> Institute of Life and Environmental Sciences, University of Tsukuba, 1-1-1 Tennodai, Tsukuba 305-8572, Ibaraki, Japan; sugimoto.takuya.gn@u.tsukuba.ac.jp

\* Correspondence: kobayashi.moto.fp@u.tsukuba.ac.jp

**Abstract:** To clarify the effect of proteins on the charging and aggregation–dispersion characteristics of oxidized carbon nanohorn (CNHox), we measured the electrophoretic mobility and stability ratios as a function of concentrations of a model protein, lysozyme (LSZ), and KCl. The zeta potential from the electrophoretic mobility of CNHox was neutralized and reversed by the addition of oppositely charged LSZ. Electrical and hydrophobic interactions between CNHox and LSZ can be attributed to the adsorption and charge reversal of CNHox. The stability ratio of CNHox in the presence or absence of LSZ showed Derjaguin–Landau and Verwey–Overbeek (DLVO) theory-like behavior. That is, the slow aggregation regime, fast aggregation regime, and critical coagulation concentration (CCC) were identified. At the isoelectric point, only the fast aggregation regime was shown. The existence of patch-charge attraction due to the charge heterogeneity on the surface was inferred to have happened due to the enhanced aggregation of CNHox at high LSZ dosage and low electrolyte concentration. The relationship between critical coagulation ionic strength and surface charge density at low LSZ dosage showed that the aggregation of CNHox is in line with the DLVO theory. An obvious decrement in the Hamaker constant at high LSZ dosage can probably be found due to an increased interaction of LSZ-covered parts.

**Keywords:** dynamic light scattering; electrophoretic mobility; non-DLVO interaction; patch-charge attraction



**Citation:** Tian, Z.; Li, M.; Sugimoto, T.; Kobayashi, M. The Effect of Lysozyme on the Aggregation and Charging of Oxidized Carbon Nanohorn (CNHox) in Aqueous Solution. *Appl. Sci.* **2024**, *14*, 2645. <https://doi.org/10.3390/app14062645>

Academic Editors: Grządka Elżbieta and Jakub Matusiak

Received: 11 February 2024

Revised: 10 March 2024

Accepted: 19 March 2024

Published: 21 March 2024



**Copyright:** © 2024 by the authors. Licensee MDPI, Basel, Switzerland. This article is an open access article distributed under the terms and conditions of the Creative Commons Attribution (CC BY) license (<https://creativecommons.org/licenses/by/4.0/>).

## 1. Introduction

Carbon nanomaterials (CNMs) have brought many new possibilities to human beings since their invention. CNMs, such as carbon nanotubes (CNTs), graphene, and carbon nanohorn (CNH), can be widely used in industry, pharmacy, and other fields such as water treatment, plant growth control, and AIDS treatment [1–5].

Nowadays, with the development of nanotechnology and the extension of human activity, the number of artificial nanomaterials released to the environment has increased in the last two decades. In this sense, the fate and transport of engineered nanoparticles are studied extensively [6,7]. The existence of colloidal nanoparticles will change the fate and facilitate the transport of heavy metal pollutants, pathogens, etc., due to aggregation and co-transport [8–10]. The different transport behaviors of nanoparticles in porous media at different pH or electrolyte conditions have also been reported [11,12]. Cations and anions, which exist widely in natural surface water, can reduce the energy barrier of colloidal systems and induce aggregation [13]. The charging behavior of particles can also change the aggregation of nanoparticles [14–16] and may also affect their transport in groundwater [17]. Therefore, the aggregation and charging of colloidal particles in different systems needs more attention.

Ever since the carbon nanohorn (CNH) was invented by Iijima et al. [18], it has received extensive attention because it possesses a large specific surface area and high conductivity.

A CNH can be produced by using  $\text{CO}_2$  laser ablation of carbon at room temperature, and the product is a powder formed of graphitic particles with an average size of approximately 100 nm [18]. Oxidized carbon nanohorns (CNHoxs) were prepared with hydrogen peroxide treatment of the CNH. Figure 1 depicts a schematic diagram of the oxidation of a CNH. In the process of the oxidation, the tips of the CNH are opened, and some charged hydrophilic carboxyl groups ( $\text{COO}^-$ ) are introduced; the porous structure allows molecules to access the inside of the CNHox and results in a larger specific surface area than a CNH.

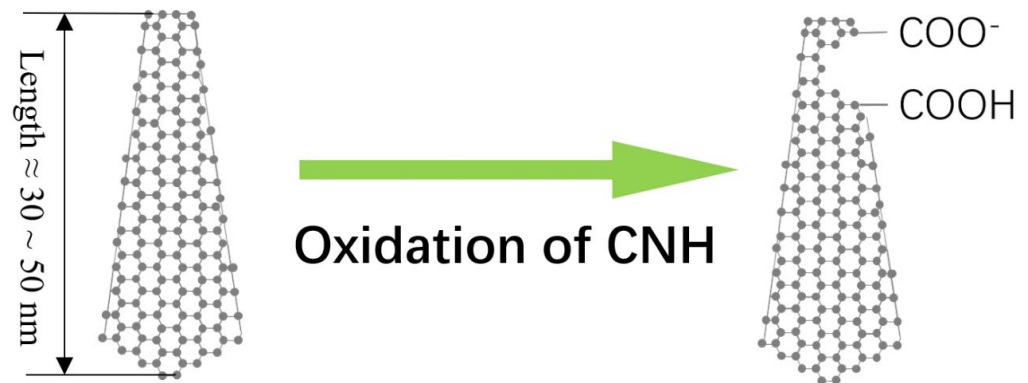


**Figure 1.** Schematic diagram of the oxidation of a CNH.

Figure 2 shows a transmission electron microscope (TEM) image of CNHox particles. This figure demonstrates that a single CNHox aggregate has a spherical structure, and that the mean diameter of CNHox aggregates is  $96 \pm 20$  nm [15].

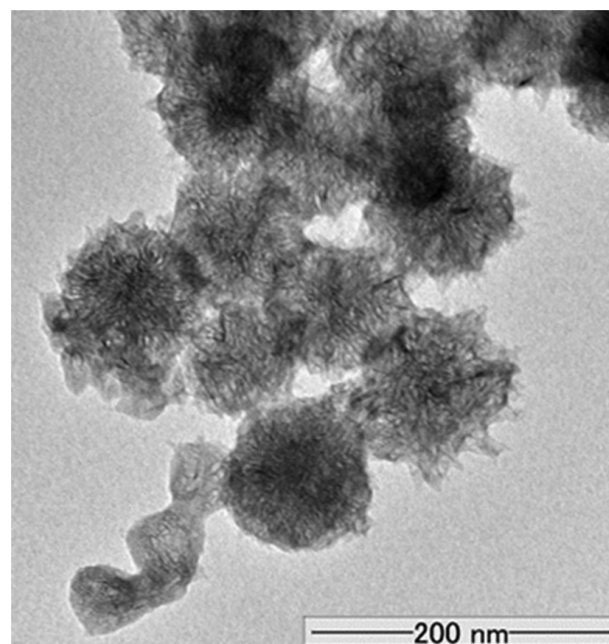


**Figure 2.** Transmission electron micrograph images of CNHox particles [15] reused with permission from Elsevier. Irreversible aggregates of CNHox of approximately 100 nm can be seen.

To gain a better understanding of the aggregation–dispersion behaviors of colloidal particles, the classical Derjaguin–Landau–Verwey–Overbeek (DLVO) theory is usually employed by introducing only two forces, say, attractive van der Waals and repulsive electrical double-layer forces [19–21]. Colloidal systems, which follow the DLVO theory, show a slow aggregation regime, fast aggregation regime, and a critical coagulation concentration (CCC) between them. The aggregation rate increases with the electrolyte concentration in

the slow aggregation regime. The aggregation rate reaches a plateau in the fast aggregation regime. Many research works about the aggregation of colloids or nanoparticles, such as polystyrene latex [22], Stöber-type silica [23], and allophane [24], have been carried out and have proved that their aggregation behaviors follow the prediction of the DLVO theory. Although CNHox particles have a complex structure which contains a horn-shape single structure and a porous structure on their surface, the aggregation behaviors of bare CNHoxs in simple salt solutions were proved to follow the DLVO theory [15]. The addition of substances such as multivalent ions, polyelectrolytes, and surfactants, which possess high opposite charges, can induce the screening of a double layer or even charge neutralization [25–27]. When charge neutralization happens, the colloidal surface has net charge close to zero. The electrical double layer repulsion disappears and van der Waals attraction will be dominant in the interaction between particles, where the colloidal particles aggregate fast.

Although the DLVO theory can be used in many colloidal systems, the existence of non-DLVO effects is well known. Due to the adsorption of oppositely charged substances, some patches with a different sign of charge appear. The adsorption of small amounts of oppositely charged substances will increase the heterogeneity on the particle surface. Therefore, patch-charge attraction happens. Electrical attraction will appear between the oppositely charged surfaces. This attraction can be affected by electrolyte concentration, macromolecule dosage, molecular masses, etc. [15,26,28]. A heterogeneously charged surface will have a larger patch-charge attraction than a homogeneously charged surface. Not only can synthetic polyelectrolytes lead to non-DLVO interaction, but the effect of natural macromolecules, such as proteins and humic substances, also need more attention. Huang et al. [23] have claimed that a low amount of adsorbed lysozyme (LSZ) promotes the aggregation of silica particles due to charge heterogeneity. The bridging effect plays an important role in the aggregation of silica particles in the presence of Suwannee River fulvic acid [29]. Saleh et al. have studied the initial aggregation kinetics of single-walled carbon nanotubes in the presence of natural organic matter, Suwannee River acid, bovine serum albumin, etc. [30].

While considering the fate and transport of colloidal particles, we cannot ignore some of the potential problems that the wide usage of CNHoxs may bring to the nanostructures of organism bodies. How a CNHox interacts with natural organic materials is highly discussed in many research studies. In previous studies, the biotoxicity of CNHoxs was proved by lots of researchers. Zieba et al. have studied the biotoxicity of CNHoxs on human cells [31]. Their result concluded that CNHoxs oxidized for 0.5 h have the highest toxicity, and thus the lowest cell viability. The effect of CNHox on the hatching rate and survival rate of zebrafish was also studied by D'amora et al., who have stated that the hatching rate and survival rate of zebrafish can be decreased by the addition of CNHoxs [32].

However, there is still a lack of research on the charging and aggregation–dispersion behaviors of CNHoxs with biological and environmental macromolecules such as proteins, polysaccharides, and humic substances, which are ubiquitous in natural environments. In previous research, the effects of high oppositely charged natural macromolecular materials on some colloidal particles' surface have been studied [23,26]. If a CNHox is to be widely used in industrial production, the interaction between CNHoxs and proteins will be also non-negligible. Therefore, clarifying how proteins affect the aggregation and dispersion of CNHoxs in aqueous solution and the applicability of the DLVO theory are of great importance.

In this study, the well-known model protein lysozyme (LSZ), which has been generally studied for its co-flocculation with many colloidal particles [23], is employed as model a protein. The charging and aggregation behaviors of CNHoxs in the presence of LSZ are studied to gain a better insight into the colloidal stability of CNHoxs in the presence of proteins. Non-DLVO interactions such as patch-charge attraction are concerned in this explanation of the aggregation–dispersion behavior of CNHox particles with protein molecules. With the usage of electrophoretic light scattering and time-resolved dynamic

light scattering methods, the charging and aggregation–dispersion of CNHoxs are explored. The results obtained will be analyzed based on the DLVO theory.

## 2. Materials and Methods

The aggregation behavior and charging behavior of CNHox nanoparticles with or without the existence of LSZ were studied by using the dynamic light scattering method (DLS) and electrophoretic light scattering method (ELS). In this research, samples varied in the quantity of additional LSZ and in electrolyte concentration without pH adjustment.

### 2.1. Materials

The oxidized carbon nanohorn (CNHox) used throughout whole of this research was produced by NEC Corporation (Tokyo, Japan). Zhang et al. [33] have demonstrated that the oxidation of CNH with hydrogen peroxide at 100 °C is an efficient way to manufacture a CNHox. Carboxyl groups are introduced and can mostly be found at the opened tips or bottoms of the horn-shape structure [33]. Then, the specific surface area of the CNHox can be increased from 400 m<sup>2</sup>/g for the raw CNH to nearly 1720 m<sup>2</sup>/g [34].

KCl (JIS special grade) from Fuji Film Wako Pure Chemical Industry (Osaka, Japan) was dissolved in deionized water to prepare electrolyte solutions with different concentrations. Then, the prepared KCl solutions were filtered with the usage of a syringe filter (DISMIC-25HP, ADVANTEC, Tokyo, Japan) with a pore size of 0.20 μm to remove particulate matters.

Hen egg-white lysozyme (LSZ) from SigmaAldrich (L6876-10G, Merck KGaA, Darmstadt, Germany) was used as a model protein. The shape of lysozyme looks like a spheroid with lengths of 3, 3, and 4.5 nm, and its molecular weight is 14.3 kDa. Furthermore, 5 g/mL of lysozyme solution was prepared as a stock solution. Proteins are amphoteric substances, which means that they can be positively or negatively charged depending on different solution conditions. Lysozyme was proved to be positively charged at pH levels below 10 [35]. Information on LSZ can be found in many previous studies [36,37]. All the LSZ solutions prepared were used up or renewed within two weeks. The LSZ solutions prepared for storage were filtered with a syringe filter (DISMIC-25HP, ADVANTEC, Tokyo, Japan) with a pore size of 0.20 μm to avoid the contamination of particulate matters.

A pH meter (ELP-035, TOA DKK Ltd., Tokyo, Japan) was used to measure the pH throughout the whole experiment. Without pH adjustment, the average pH in this experiment was 5.59 ± 0.34. All the water used was deionized by using the Elix purification system. All the experiments were carried out under conditions of 20 °C.

### 2.2. Method

#### 2.2.1. Electrophoretic Mobility

We measured the electrophoretic mobilities (EPMs) of CNHoxs at different KCl and LSZ concentrations. The CNHox suspension used was dispersed with an ultrasonic disperser (US-2R, AS ONE Corporation, Osaka, Japan) to maintain an evenly dispersed suspension. All the samples were prepared with a CNHox concentration of 2 mg/L and a volume of 10 mL by mixing prescribed volumes of KCl solution, HCl or KOH solution, CNHox suspension, and de-ionized water. A capillary cell (DTS1070, Malvern Panalytical Ltd., Malvern, UK) was prewashed three times by using the sample after the preparation for each measurement. Then, each of the samples was injected into the capillary cell. The cell was inserted into a Zetasizer Nano-ZS (Malvern Panalytical Ltd, Malvern, UK) and the EPM was subsequently measured by using electrophoretic light scattering. The EPM was measured as soon as evenly mixed samples were prepared. The EPM measurements were carried out three times and completed within 5 min. The condition that  $\kappa a > 1$  for irreversible CNHox aggregates was satisfied [38], where  $\kappa^{-1}$  is the thickness of the electric double layer ~30 nm at 0.1 mM and  $a$  is the radius of the CNHox aggregates ~100 nm. The

flow in the pore of the CNHox was regarded as negligible. Therefore, the zeta potential  $\zeta$  can be reasonably obtained by using Smoluchowski's equation as follows:

$$\mu = \frac{\varepsilon_0 \varepsilon_r \zeta}{\eta}, \quad (1)$$

$\mu$  is the EPM,  $\varepsilon_0$  is permittivity of the vacuum,  $\varepsilon_r$  is the relative dielectric constant of the water, and  $\eta$  is viscosity of the solution.

### 2.2.2. Dynamic Light Scattering

The dynamic light scattering method (DLS) was used to investigate the aggregation behavior of the CNHox with various electrolyte concentrations and different amounts of LSZ. The used CNHox suspension was dispersed with an ultrasonic disperser (US-2R, AS ONE Corporation) to disperse the aggregates. Each sample had a total volume of 1 mL with a CNHox concentration of 2 mg/L in a disposable polystyrene cell. Appropriate amounts of the CNHox suspension, deionized water, KCl solution, and LSZ solution were added into the disposable polystyrene cell. All the disposable polystyrene cells used were cleaned by soaking them in NaOH (0.1 M) solution, HCl (0.1 M) solution, and deionized water in that order. After the preparations, each sample in the cell was immediately shaken with a mixer (MVM-10, AS ONE Corporation, Osaka, Japan). Then, the time-resolved dynamic light scattering (DLS) method (Zetasizer Nano-ZS, Malvern Panalytical Ltd, Malvern, UK) was carried out and the temporal change in hydrodynamic size was measured. The results of average hydrodynamic diameter ( $d_h$ ) as a function of time ( $t$ ) were obtained.

The relationship between the  $d_h$  of aggregates and the particles' diffusion coefficient ( $D$ ) was related by Stokes–Einstein equation:

$$d_h = \frac{k_B T}{3\pi\eta D}, \quad (2)$$

where  $k_B$  is the Boltzmann constant,  $T$  is the absolute temperature, and  $\eta$  is the dynamic viscosity. From the relationship between  $d_h$  and time ( $t$ ), the initial increased rate of the hydrodynamic diameter  $(dd_h/dt)_{t \rightarrow 0}$  corresponds to the apparent aggregation rate in this experiment, also known as the initial slope. The relationship between the measured particle size and time was fitted with a 3rd order polynomial equation, and the coefficient of the 1st order term in the equation was extracted to represent the initial slope  $(dd_h/dt)_{t \rightarrow 0}$ . The measurements were performed by varying the concentrations of the KCl and LSZ. All the measured values of  $(dd_h/dt)_{t \rightarrow 0}$  were normalized to the rate  $(dd_h/dt)_{t \rightarrow 0}^f$  of the fast aggregation regime, where the van der Waals attraction is dominant. The normalized rates can be related to the stability ratio  $W$ , defined as follows:

$$W = \frac{(dd_h/dt)_{t \rightarrow 0}^f}{(dd_h/dt)_{t \rightarrow 0}}, \quad (3)$$

The normalized rates are equal to the reciprocal stability ratio ( $1/W$ ). We evaluated the reciprocal stability ratio ( $1/W$ ) as a function of KCl concentration with/without LSZ. From the results of the reciprocal stability ratio we extracted the critical coagulation concentration (CCC), which is an important measure for distinguishing whether aggregation occurred in a fast or slow regime since the CCCs divide the two regimes [15,16,24,39].

## 3. Results and Discussion

### 3.1. Charging Behavior of Bare CNHox

We plotted the experimental zeta potentials of the CNHox against the KCl concentrations, as depicted in Figure 3. The zeta potentials were converted from the measured EPMS using Smoluchowski's equation (Equation (1)). Each of the points shows the average value

of a total of three measurements. The error bars are used to show the standard deviation for each case.

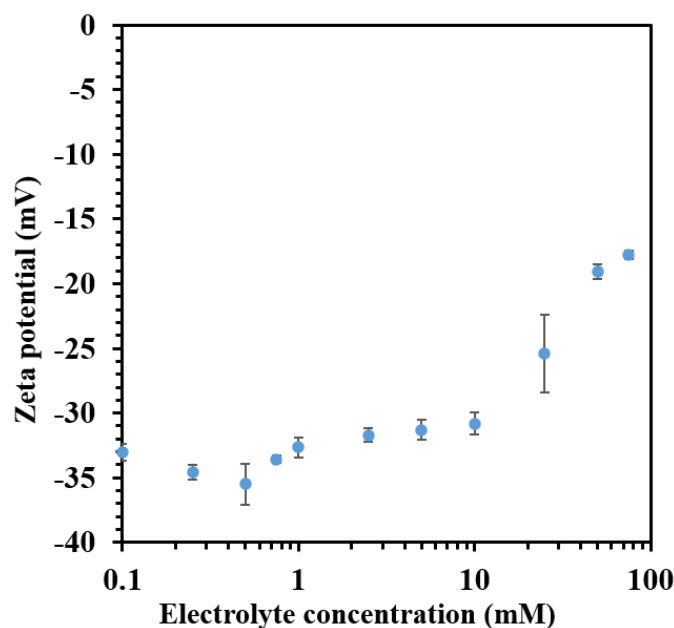


**Figure 3.** The relationship between the zeta potential of the CNHox and KCl concentration.

Figure 3 demonstrates that the CNHox is negatively charged in KCl solutions. The surface of the CNHox has carboxyl groups because of oxidation [18]. Due to the deprotonation of the carboxyl groups, this group can account for the negative charge on the CNHox surface. As the KCl concentration increases, the EPM remains negative in this range but decreases in magnitude, say, charge reversal does not happen. The reason why the magnitude of the zeta potential decreases may be attributed to the electrical double-layer (EDL) screening caused by the increment in KCl concentration. The compression of EDL due to high counterion concentration leads to lower magnitudes of zeta potential.

### 3.2. Aggregation Behavior of Bare CNHox

Figure 4 depicts the temporal variations in the hydrodynamic diameter of the CNHox ( $d_h$ ) at different KCl concentrations. According to Figure 4, the CNHox diameter ( $d_h$ ) grows with time because of aggregation at higher salt concentrations. The initial slope in  $d_h$  vs.  $t$  increases when the amount of salt increases. Above a certain salt concentration, in this case, 25 mM, the slopes do not noticeably alter.

In Figure 5, the reciprocal stability ratio  $1/W$  is plotted against the KCl concentration after arranging the initial slope  $(dd_h/dt)_{t \rightarrow 0}$  at different electrolyte concentrations. The measurement of temporal hydrodynamic change was carried out three times at each electrolyte concentration. In this picture, we can clearly distinguish the slow aggregation regime and the fast aggregation regime, and the critical point called the critical coagulation concentration (CCC). The experimental data, denoted as the blue filled circles, show that the  $1/W$  increases as the KCl concentration increases and then reaches a constant value, where enters the fast aggregation regime. From the DLVO theory, we can consider that in the increment process of  $1/W$  with KCl concentration, the surface charge of the CNHox is screened by the counterion in varying degrees and the van der Waals force gradually dominates this process relative to the double-layer interaction. The electric double layer undergoes stronger suppression while the electrolyte concentration becomes higher. The aggregation can be attributed to the van der Waals attraction. According to Figure 5, the reciprocal stability ratio rises and reaches unity as the KCl concentration is increased. By fitting the experimental data with the empirical function [40] (Equation (4))

$$\frac{1}{W} = \frac{1}{1 + \left(\frac{CCC}{C_s}\right)^\beta} \quad (4)$$

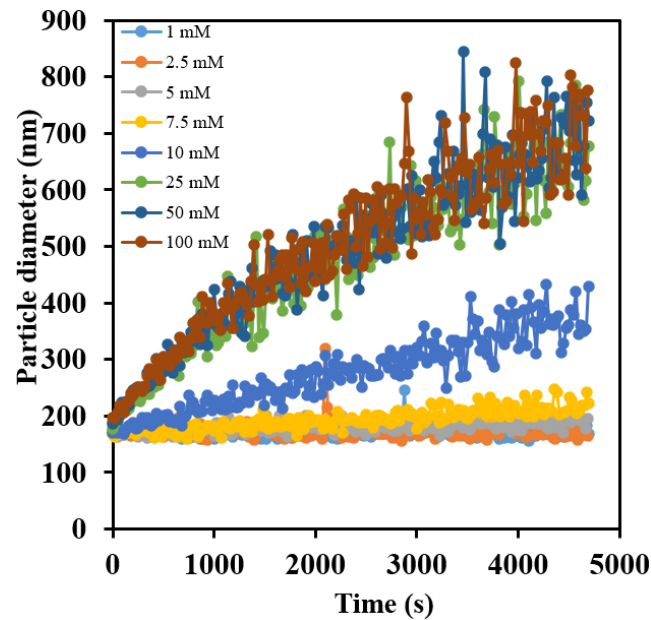


**Figure 4.** Hydrodynamic diameter of bare CNHox particles as a function of time at different KCl concentrations.

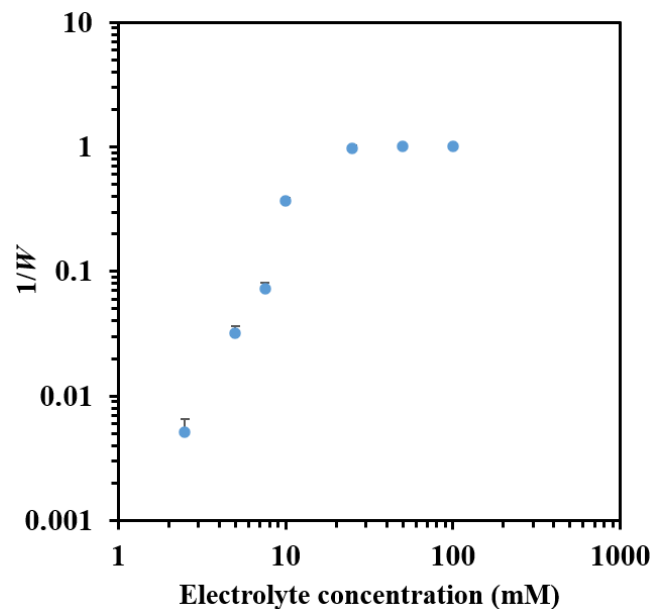


**Figure 5.** The reciprocal stability ratio  $1/W$  of CNHox as a function of KCl concentration.

We can find that the CCC is 11.44 mM, which is in good agreement with the previous research [15]. Although the CNHox has a relatively complex structure compared to spherical particles such as polystyrene latex, the aggregation behavior of the CNHox looks similar [16,22,24,39].

### 3.3. Effect of LSZ on the Charging Behavior of CNHox

The electrophoretic mobility of the CNHox in the presence of different concentrations of LSZ was measured to corroborate the charging behavior, and Equation (1) was used to determine the zeta potential. According to the manufacturer of Zetasizer Nano-ZS (Malvern, Australia), the detection limit of EPM for a protein of 15 kDa is 1 g/L. Therefore, the scattering from LSZ might be negligible. KCl was used as a background electrolyte and had a concentration of 10 mM after mixing. The lysozyme concentration ranged from 0.001 mg/L to 1 g/L, whereas the concentration of the CNHox was fixed at 2 mg/L.

In Figure 6, each of the filled blue circles stands for the zeta potential at different mass ratio values of LSZ to CNHox. The magnitude of the zeta potential reduces somewhat as the mass ratio rises and reaches the isoelectric point (IEP) at about 0.0875 g/g. The charge reversal occurs with a steep slope as the mass ratio increases. For the IEP at a higher mass ratio of LSZ to CNHox, the slope gradually closes to zero where the mass ratio is around 50 g/g. Then, the low mass ratio, IEP, and high mass ratio can be determined from this result. These charging behaviors result from the adsorption of positively charged LSZ to the negatively charged CNHox surface. This behavior acts similarly to the neutralization and charge reversal of natural clay allophane and silica by counterions and LSZ, respectively [16,23,24,39]. Wei et al. [41] have simulated the adsorption of LSZ on hydrophobic surfaces and declared that LSZ can be adsorbed on a hydrophobic surface unless the interaction energy between protein and surface is strong enough to break the hydration shell barrier. Not only does the orientation of LSZ molecules relative to the hydrophobic surface play a part, but the attractive hydrophobic interaction plays a non-negligible role [42] in the adsorption of LSZ on a hydrophobic surface; one can also assume that these factors contribute to the strong charge reversal at high LSZ concentrations.

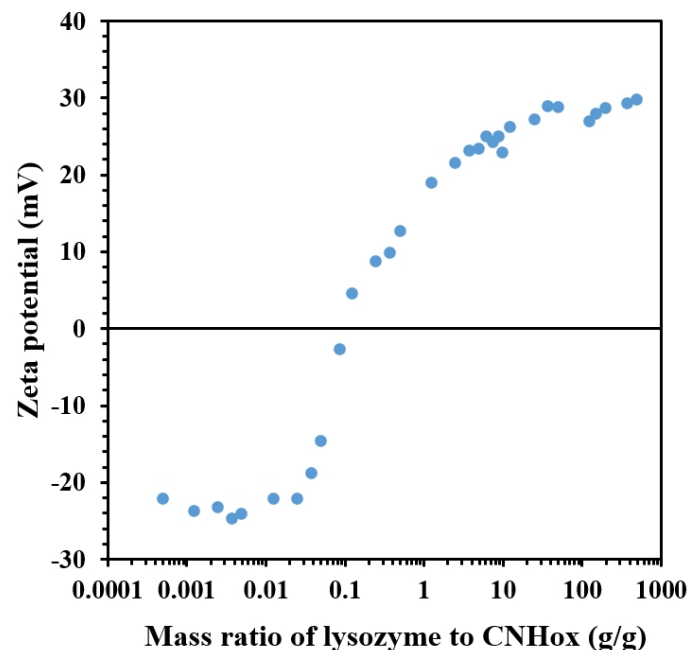


**Figure 6.** Zeta potential of lysozyme-coated CNHox in 10 mM KCl as a function of the mass ratio of lysozyme to CNHox (g/g).

Although we found the charge reversal and the saturation point, the adsorption amount of LSZ and whether or not the LSZ can enter in the cavity of CNHox are still unclear.

### 3.4. Effect of LSZ on the Aggregation Behavior of CNHox

Figure 7 displays the temporal variations in the hydrodynamic diameter ( $d_h$ ) of lysozyme-coated CNHox at various mass ratios. The pH in this experiment was  $5.65 \pm 0.32$  without making any pH adjustment. In Figure 7, the circles filled in different colors

stand for different KCl concentrations. The initial slopes  $(dd_h/dt)_{t \rightarrow 0}$  do not make a big difference in each case in Figure 7a compared with Figure 3. This result implies that all the negative charge on surface of CNHox is neutralized by the positively charged lysozyme. The interaction between CNHox particles is dominated by van der Waals attraction rather than electric repulsive force. This interaction leads to a fast aggregation rate in a large range of electrolyte concentrations. We also cannot ignore that although the initial slope in each case is almost the same, higher electrolyte concentrations lead to particle diameter changes more quickly. This may be due to the screening effect.

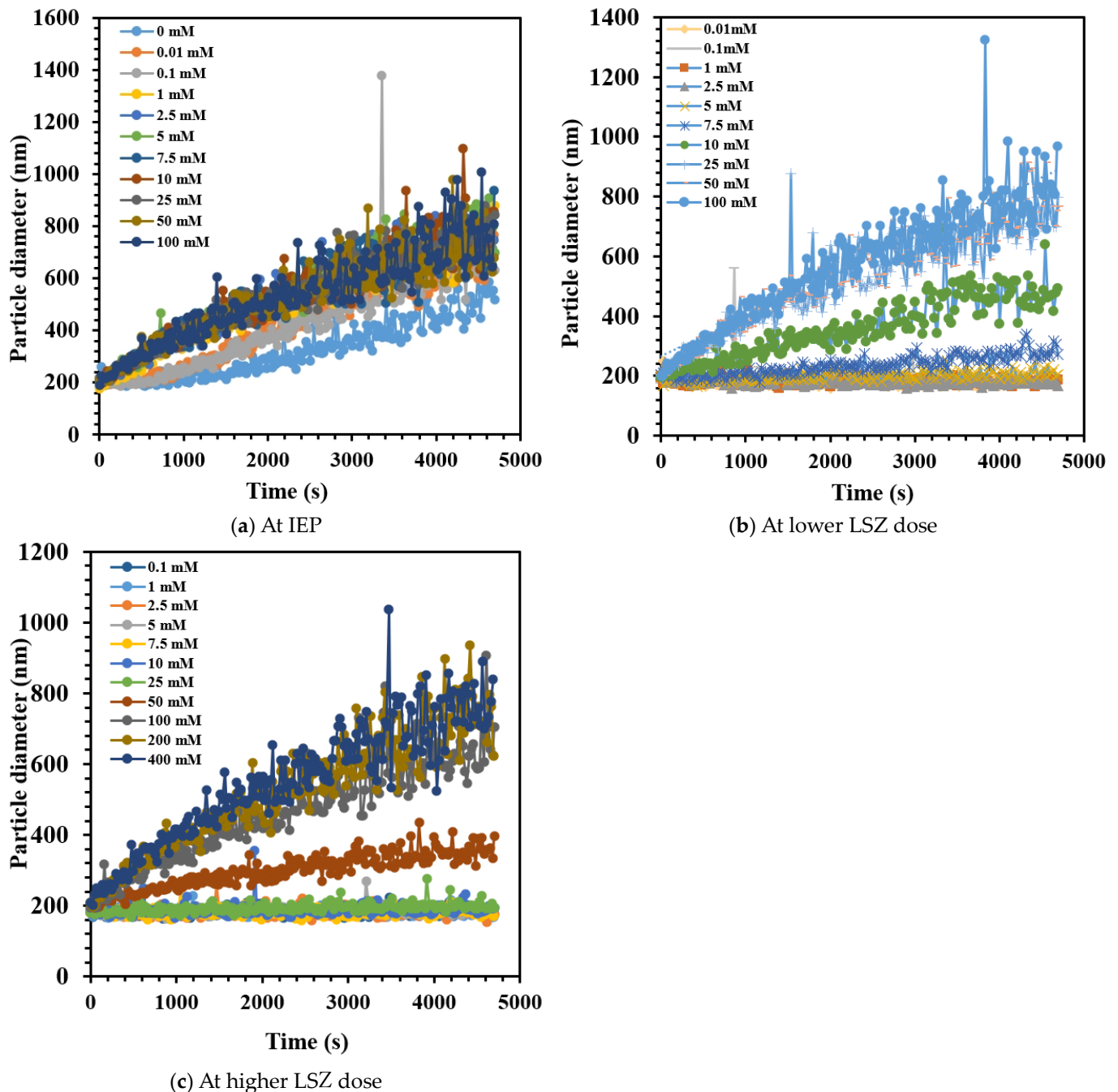


**Figure 7.** Hydrodynamic diameter changes in lysozyme-coated CNHox particles with time for the mass ratios of (a) 0.0875 g/g, (b) 0.01 g/g, and (c) 50 g/g and various KCl concentrations.

Figure 7b,c shows almost same trend in particle diameter changes, but apparently a higher electrolyte concentration is needed to reach the CCC at a mass ratio of 50 g/g; one

can assume this can be attributed to the relatively higher surface charge density. Details will be discussed in Figure 8.

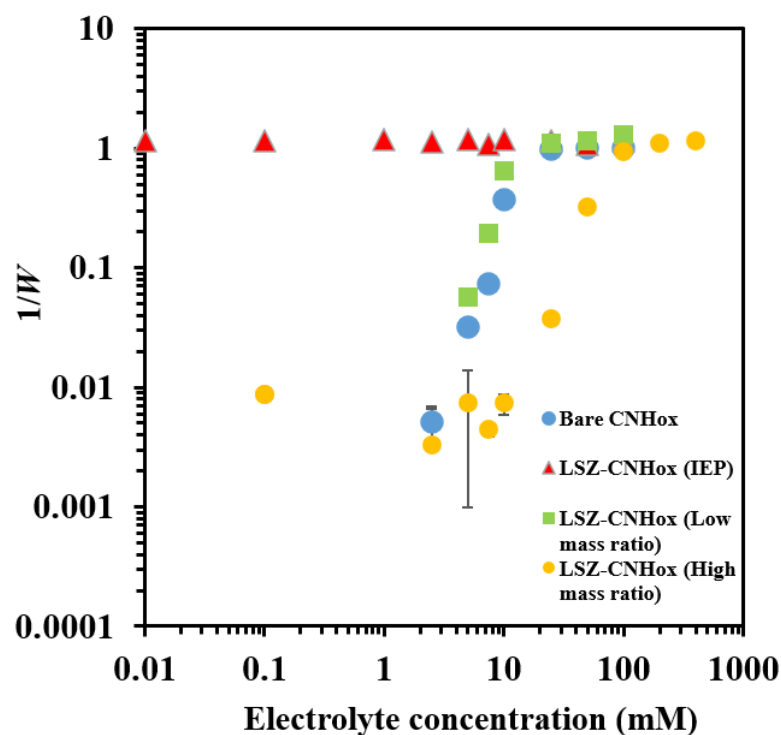


**Figure 8.** Reciprocal stability ratio  $1/W$  against KCl concentration for bare CNHox (blue circles), CNHox with LSZ at the IEP (red triangles), CNHox with LSZ at low mass ratio (green squares), and CNHox with LSZ at high mass ratio (yellow circles).

The different symbols in Figure 8 represent the data collected at various LSZ/CNHox mass ratios. The aggregation behaviors of the CNHox with LSZ are also DLVO-like. The addition of LSZ with a mass ratio of 0.0875 g/g decreases the CCC and dramatically induces aggregation, and low-to-high salt concentrations exist in the fast aggregation regime at the IEP. This can be attributed to the fact that the coated lysozyme neutralizes the negatively charged CNHox surface. The aggregation rates were unaffected by the salt concentration at the IEP, where the  $1/W$  was almost unified. In the case of a high dose of LSZ (50 g/g), the increment in CCC to 60.53 mM proves the larger magnitude of the zeta potential due to the charge reversal. It is possible to explain the unexpected increase in  $1/W$  at the low electrolyte concentration by the presence of a non-DLVO attractive force; during the charge neutralization and the charge reversal of CNHox, the adsorption of LSZ causes the surface charge to become heterogenous (shown in Figure 9). In the conditions of bare CNHox with trivalent counterions, patch-charge attraction was also observed [15]. This phenomenon is also usually discussed in the study of polyelectrolytes [28].

We also need to pay attention to the fact that salt dependence in the slow aggregation regime at a high mass ratio is slightly weaker than in cases at a low mass ratio and without additional LSZ. However, in the DLVO theory, the slope of stability plots should be barely changed at different the electrolyte concentrations [43]. Therefore, the slightly gentle slope observed at a high mass ratio in this study implies the existence of a non-DLVO force due to heterogeneity.

Molina-Bolívar et al. [44] have proved that the hydrophobicity and hydrophilicity can be attributed to the efficiency of colloidal stabilization. In the meanwhile, proteins tend to expose most hydrophilic areas in aqueous solution. The hydration force, therefore, plays a significant role in the aggregation at a high mass ratio of 50 g/g, contributing to the high CCC.

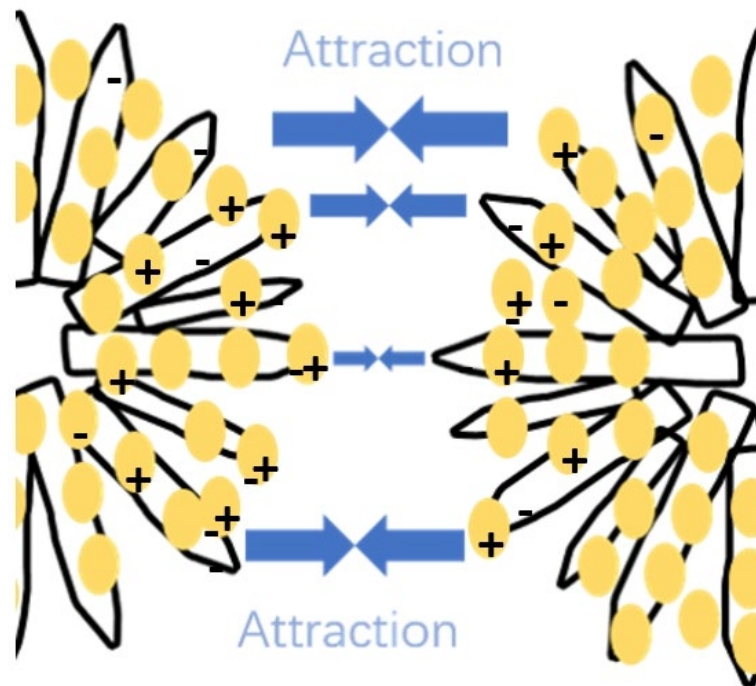


Figure 9. Sketch map of patch-charge attraction between two LSZ-saturated CNHox particles.

Compared with the yellow solid circles at 0.1 mM and 5 mM in Figure 8, as the electrolyte concentration increases, more counterion is adsorbed on the saturated lysozyme layer and then the surface becomes less heterogenous. This could explain the decrease in  $1/W$  at low electrolyte concentrations. Borkovec et al. [45] have also found a change in slope while plotting the stability ratio, and they claimed that the charging heterogeneity on the surface of colloidal particles can be attributed to the non-DLVO forces. The more heterogeneously charged the surface is, the more obvious the gradual slope is; the patch-charge attraction plays a more important role between more heterogeneously charged surfaces.

### 3.5. Comparison between Experimental Data and DLVO Prediction

Trefalt et al. [46] have demonstrated the following relationship between critical coagulation ionic strength (CCIS) and surface charge density ( $\sigma$ ) from the DLVO theory:

$$CCIS = \left( \frac{9}{8\pi \exp(2)} \right)^{\frac{1}{3}} \frac{1}{\lambda_B} \left( \frac{\sigma^2}{\epsilon_0 \epsilon_r H} \right)^{\frac{2}{3}}, \tag{5}$$

where  $H$  is the Hamaker constant, which characterizes the magnitude of van der Waals interaction potential between particles;  $\epsilon_0 \epsilon_r$  is the dielectric constant; and  $\lambda_B$  is the Bjerrum length, which can be calculated with Equation (6):

$$\lambda_B = \frac{e^2}{4\pi k_B T \epsilon_0 \epsilon_r}, \tag{6}$$

where  $e$  is the elementary charge. Within the Debye–Hückel approximation, the surface charge density  $\sigma$  can be calculated with Equation (7):

$$\sigma = \epsilon_0 \epsilon_r \kappa \psi_{dl}, \tag{7}$$

where the diffuse layer potential  $\psi_{dl}$  is roughly equivalent to the zeta potential, and  $\kappa^{-1}$  is the Debye length, which corresponds to the thickness of the diffuse double layer.

$$\kappa^{-1} = \left( \frac{\epsilon_0 \epsilon_r k_B T}{2 N_A e^2 I} \right)^{\frac{1}{2}}, \tag{8}$$

where  $I$  is the ionic strength, which can be calculated with Equation (9):

$$I = \frac{1}{2} \sum_i z_i^2 c_i, \tag{9}$$

where  $z_i$  is the  $i$ -th ion valence, and  $c_i$  is the concentration of  $i$ -th ion.

The correlation between the surface charge density and CCIS of CNHoxs in the presence of LSZ is depicted in Figure 10. The experimental data of the CNHox in the presence of LSZ are represented by the red filled circles. The broken dotted line, dashed line, solid line, and broken line correspond to the DLVO predictions with Hamaker constants of  $4 \times 10^{-21}$  J,  $1 \times 10^{-20}$  J,  $2 \times 10^{-20}$  J, and  $7 \times 10^{-20}$  J, respectively. The experimental result from Omija et al. [15] (open triangle) and the experimental result of this research (red filled circles) are well aligned with the theoretical DLVO prediction. The DLVO theory works very well with bare CNHox and CNHox in the presence of LSZ. These four chosen Hamaker constants cover the results from Omija et al. [15] and this research.

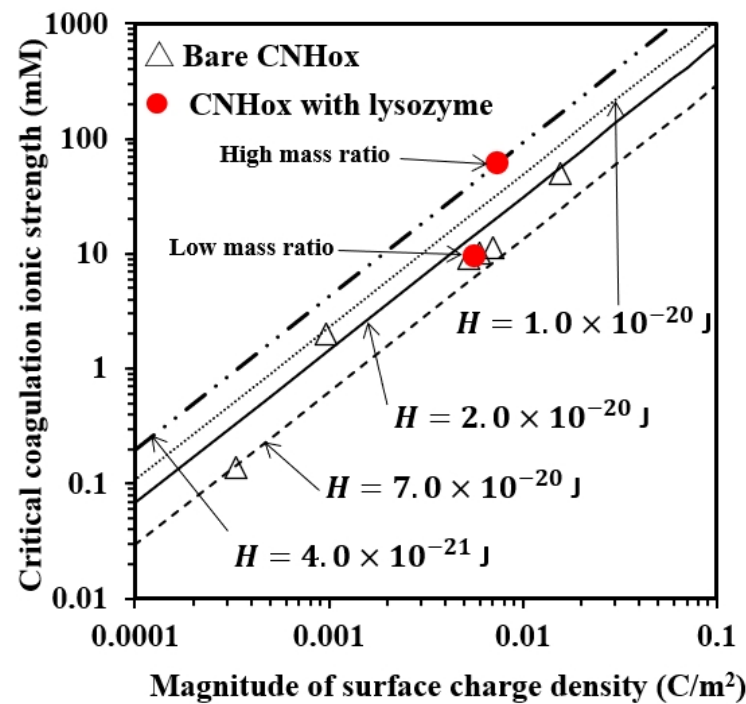


**Figure 10.** Comparison between surface charge density ( $\sigma$ ) of LSZ-coated CNHox (red filled circles), bare CNHox [15] (white open triangle), and critical coagulation ionic strength (CCIS) with DLVO prediction with different Hamaker constant  $H$  (dash-dot line, solid line, dotted line, and broken line).

In Figure 10, the result of the CNHox at a high mass ratio is located at the calculated line with a relatively lower Hamaker constant ( $4 \times 10^{-21}$  J), which is well-aligned with the result calculated by Blomberg et al. [47] for a  $3.3 \times 10^{-21}$  J Hamaker constant of LSZ–water–LSZ. This phenomenon indicates that the attractive interaction between the LSZ–water–LSZ is smaller than that of CNHox–water–CNHox.

The zeta potentials at different mass ratios as a function of electrolyte concentration are depicted in Figure 11. In the case of bare CNHox and a low mass ratio, the results are not much different. The adsorption of a small amount of LSZ slightly reduces the net

charge compared with bare CNHox; at a high mass ratio, CCC shifts to a relatively higher electrolyte concentration and a lower magnitude of zeta potential, and this agrees with the outcome depicted in Figure 11. The magnitude of zeta potential, in this case, reaches 40 mV, which is the largest without an additional electrolyte compared to the other cases. It should be noted that the magnitude of the zeta potential with a high mass ratio at CCC is significantly smaller than for bare CNHox and for CNHox coated with a low amount of LSZ. This phenomenon indicates the presence of additional non-DLVO repulsion. Huang et al. [23] have stated that the saturated LSZ layer inhibits the aggregation of silica particles. Li et al. [14] have also proved that the existence of a “BSA corona crown” adsorbed on the surface of the colloidal particles can significantly inhibit the aggregation. In this experiment, the shift in CCC to a higher value may also be attributed to the same reason, that is, the existence of steric repulsion or a lower Hamaker constant between LSZ-saturated layers. However, comparing CNHox with silica, the former has a more complex structure than the latter, and there is still a need for more studies in this orientation.

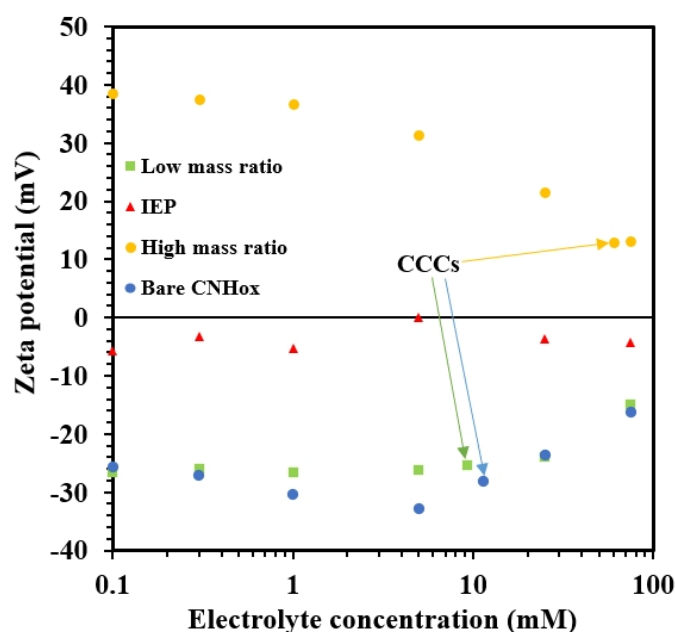


**Figure 11.** Zeta potential of bare CNHox or CNHox with the presence of LSZ at different mass ratios depending on the electrolyte concentration.

DLVO and non-DLVO interactions play important roles in the stability and assembly of colloidal particles [48]. Based on the classical DLVO theory, van der Waals attraction and electrical double-layer repulsion act together on the aggregation and dispersion of CNHoxs in the presence of LSZ. According to Figures 8 and 11, van der Waals attraction is dominant in the interaction between CNHox particles at high electrolyte concentrations due to the suppression of the electrical double layer. Meanwhile, electrical double-layer repulsion is dominant in the interaction at low electrolyte concentrations. Non-DLVO interactions cannot be ignored either. According to Figure 8, non-DLVO behavior can be found at 0.1 mM and 2.5 mM at a high mass ratio due to the charge heterogeneity on the CNHox surface. At a high mass ratio around the CCC, the calculated Hamaker constant is the smallest among other conditions, and the magnitude of zeta potential is also the smallest. This result proves the existence of non-DLVO repulsion.

#### 4. Conclusions

This study investigated the charging and aggregation behaviors of oxidized carbon nanohorns (CNHoxs) in KCl solution in the presence of lysozyme (LSZ). The concentrations of KCl and LSZ were varied. The electrophoretic mobility data show that positively charged LSZ can neutralize and even reverse the net charge of CNHoxs. The presence of LSZ induces

or inhibits the aggregation of the CNHox at the IEP or a high lysozyme dose, respectively. The critical coagulation concentration (CCCs) of CNHox with LSZ shifted from that of bare CNHox under various circumstances. The outcomes of the stability ratio and correlation between the critical coagulation ionic strength and surface charge density show that the aggregation–dispersion behavior of CNHoxs in the presence of LSZ is in good accord with the DLVO theory. In the presence of a high mass ratio of LSZ, the existence of non-DLVO attraction and repulsion can affect the aggregation of CNHoxs, causing non-DLVO behavior.

**Author Contributions:** Conceptualization, M.K.; methodology, M.K.; software, Z.T. and M.K.; validation, Z.T. and M.K.; formal analysis, Z.T. and M.K.; investigation, Z.T., M.L., T.S. and M.K.; resources, M.K.; data curation, M.K.; writing—original draft preparation, Z.T. and M.K.; writing—review and editing, M.L., T.S. and M.K.; visualization, Z.T.; supervision, M.K.; project administration, M.K.; funding acquisition, M.K. All authors have read and agreed to the published version of the manuscript.

**Funding:** The authors are thankful to the financial support from JSPS KAKENHI (19H03070, 21K14939). This research was funded by JST SPRING, Grant Number JPMJSP2124.

**Data Availability Statement:** The data are available from the authors upon reasonable request.

**Acknowledgments:** The authors are thankful to kind support from Yasuhisa Adachi, as well as to the seniors for their help in this research.

**Conflicts of Interest:** The authors declare no conflicts of interest.

## References

1. Xiao, B.; Thomas, K.M. Adsorption of aqueous metal ions on oxygen and nitrogen functionalized nanoporous activated carbons. *Langmuir* **2005**, *21*, 3892–3902. [CrossRef]
2. Ajima, K.; Yudasaka, M.; Murakami, T.; Maigné, A.; Shiba, K.; Iijima, S. Carbon nanohorns as anticancer drug carriers. *Mol. Pharm.* **2005**, *2*, 475–480. [CrossRef]
3. Khodakovskaya, M.; Dervishi, E.; Mahmood, M.; Xu, Y.; Li, Z.; Watanabe, F.; Biris, A.S. Carbon nanotubes are able to penetrate plant seed coat and dramatically affect seed germination and plant growth. *ACS Nano* **2009**, *3*, 3221–3227. [CrossRef] [PubMed]
4. Tripathi, S.; Sonkar, S.K.; Sarkar, S. Growth stimulation of gram (*Cicer arietinum*) plant by water soluble carbon nanotubes. *Nanoscale* **2011**, *3*, 1176–1181. [CrossRef] [PubMed]
5. Friedman, S.H.; Decamp, D.L.; Sijbesma, R.P.; Srdanov, G.; Wudl, F.; Kenyon, J., G.L. Inhibition of the HIV-1 Protease by Fullerene Derivatives: Model Building Studies and Experimental Verification. *J. Am. Chem. Soc.* **1993**, *115*, 6506–6509. Available online: <https://pubs.acs.org/doi/pdf/10.1021/ja00068a005> (accessed on 31 January 2024). [CrossRef]
6. Praetorius, A.; Badetti, E.; Brunelli, A.; Clavier, A.; Gallego-Urrea, J.A.; Gondikas, A.; Hassellöv, M.; Hofmann, T.; Mackevica, A.; Marcomini, A.; et al. Strategies for determining heteroaggregation attachment efficiencies of engineered nanoparticles in aquatic environments. *Environ. Sci. Nano* **2020**, *7*, 351–367. [CrossRef]
7. Peijnenburg, W.J.G.M.; Baalousha, M.; Chen, J.; Chaudry, Q.; Von der Kammer, F.; Kuhlbusch, T.A.J.; Lead, J.; Nickel, C.; Quik, J.T.K.; Renker, M.; et al. A Review of the Properties and Processes Determining the Fate of Engineered Nanomaterials in the Aquatic Environment. *Crit. Rev. Environ. Sci. Technol.* **2015**, *45*, 2084–2134. [CrossRef]
8. Lin, D.; Tian, X.; Wu, F.; Xing, B. Fate and Transport of Engineered Nanomaterials in the Environment. *J. Environ. Qual.* **2010**, *39*, 1896–1908. [CrossRef]
9. Liao, P.; Pan, C.; Ding, W.; Li, W.; Yuan, S.; Fortner, J.D.; Giammar, D.E. Formation and Transport of Cr(III)-NOM-Fe Colloids upon Reaction of Cr(VI) with NOM-Fe(II) Colloids at Anoxic-Oxic Interfaces. *Environ. Sci. Technol.* **2020**, *54*, 4256–4266. [CrossRef]
10. Ling, X.; Yan, Z.; Liu, Y.; Lu, G. Transport of nanoparticles in porous media and its effects on the co-existing pollutants. *Environ. Pollut.* **2021**, *283*, 117098. [CrossRef]
11. Kumari, J.; Mathur, A.; Rajeshwari, A.; Venkatesan, A.; Satyavati, S.; Pulimi, M.; Chandrasekaran, N.; Nagarajan, R.; Mukherjee, A. Individual and co transport study of titanium dioxide NPs and zinc oxide NPs in porous media. *PLoS ONE* **2015**, *10*, e0134796. [CrossRef]
12. Jaisi, D.P.; Saleh, N.B.; Blake, R.E.; Elimelech, M. Transport of single-walled carbon nanotubes in porous media: Filtration mechanisms and reversibility. *Environ. Sci. Technol.* **2008**, *42*, 8317–8323. [CrossRef]
13. Li, X.; He, E.; Xia, B.; Van Gestel, C.A.; Peijnenburg, W.J.; Cao, X.; Qiu, H. Impact of CeO<sub>2</sub> nanoparticles on the aggregation kinetics and stability of polystyrene nanoplastics: Importance of surface functionalization and solution chemistry. *Water Res.* **2020**, *186*, 116324. [CrossRef]
14. Li, X.; He, E.; Jiang, K.; Peijnenburg, W.J.; Qiu, H. The crucial role of a protein corona in determining the aggregation kinetics and colloidal stability of polystyrene nanoplastics. *Water Res.* **2021**, *190*, 116742. [CrossRef]

15. Omija, K.; Hakim, A.; Masuda, K.; Yamaguchi, A.; Kobayashi, M. Effect of counter ion valence and pH on the aggregation and charging of oxidized carbon nanohorn (CNHox) in aqueous solution. *Colloids Surf. A Physicochem. Eng. Asp.* **2021**, *619*, 126552. [[CrossRef](#)]
16. Li, M.; Kobayashi, M. The aggregation and charging of natural clay allophane: Critical coagulation ionic strength in the presence of multivalent counter-ions. *Colloids Surf. A Physicochem. Eng. Asp.* **2021**, *626*, 127021. [[CrossRef](#)]
17. Ryan, J.N.; Elimelech, M. Colloid mobilization and transport in groundwater. *Colloids Surf. A Physicochem. Eng. Asp.* **1996**, *107*, 1–56. [[CrossRef](#)]
18. Iijima, S.; Yudasaka, M.; Yamada, R.; Bandow, S.; Suenaga, K.; Kokai, F.; Takahashi, K. Nano-aggregates of single-walled graphitic carbon nano-horns. *Chem. Phys. Lett.* **1999**, *309*, 165–170. [[CrossRef](#)]
19. Derjaguin, B.; Landau, L. Theory of the Stability of Strongly Charged Lyophobic Sols and of the Adhesion of Strongly Charged Particles in Solutions of Electrolytes. *Prog. Surf. Sci.* **1993**, *43*, 30–59. [[CrossRef](#)]
20. Verwey, E.J.; Overbeek, J.T.G. *Theory of the Stability of Lyophobic Colloids*; Elsevier Publishing Company: Amsterdam, The Netherlands, 1948.
21. Ohshima, H. *Electrical Phenomena at Interfaces and Biointerfaces*, 1st ed.; John Wiley & Sons: Hoboken, NJ, USA, 2012; Available online: [https://books.google.co.jp/books?hl=en&lr=&id=OZzi9FkNiuEC&oi=fnd&pg=PR11&ots=9g91twSkvP&sig=Kwc9mHwCCcNGh2JNsJZ6YgKxV18&redir\\_esc=y#v=onepage&q&f=false](https://books.google.co.jp/books?hl=en&lr=&id=OZzi9FkNiuEC&oi=fnd&pg=PR11&ots=9g91twSkvP&sig=Kwc9mHwCCcNGh2JNsJZ6YgKxV18&redir_esc=y#v=onepage&q&f=false) (accessed on 8 February 2024).
22. Sugimoto, T.; Cao, T.; Szilagyi, I.; Borkovec, M.; Trefalt, G. Aggregation and charging of sulfate and amidine latex particles in the presence of oxyanions. *J. Colloid Interface Sci.* **2018**, *524*, 456–464. [[CrossRef](#)]
23. Huang, Y.; Yamaguchi, A.; Pham, T.D.; Kobayashi, M. Charging and aggregation behavior of silica particles in the presence of lysozymes. *Colloid Polym. Sci.* **2018**, *296*, 145–155. [[CrossRef](#)]
24. Takeshita, C.; Masuda, K.; Kobayashi, M. The effect of monovalent anion species on the aggregation and charging of allophane clay nanoparticles. *Colloids Surf. A Physicochem. Eng. Asp.* **2019**, *577*, 103–109. [[CrossRef](#)]
25. Bharti, B.; Meissner, J.; Klapp, S.H.L.; Findenegg, G.H. Bridging interactions of proteins with silica nanoparticles: The influence of pH, ionic strength and protein concentration. *Soft Matter* **2014**, *10*, 718–728. [[CrossRef](#)]
26. Adachi, Y.; Feng, L.; Kobayashi, M. Kinetics of flocculation of polystyrene latex particles in the mixing flow induced with high charge density polycation near the isoelectric point. *Colloids Surf. A Physicochem. Eng. Asp.* **2015**, *471*, 38–44. [[CrossRef](#)]
27. Szilagyi, I.; Trefalt, G.; Tiraferri, A.; Maroni, P.; Borkovec, M. Polyelectrolyte adsorption, interparticle forces, and colloidal aggregation. *Soft Matter* **2014**, *10*, 2479–2502. [[CrossRef](#)]
28. Gillies, G.; Lin, W.; Borkovec, M. Charging and aggregation of positively charged latex particles in the presence of anionic polyelectrolytes. *J. Phys. Chem. B* **2007**, *111*, 8626–8633. [[CrossRef](#)] [[PubMed](#)]
29. Abe, T.; Kobayashi, S.; Kobayashi, M. Aggregation of colloidal silica particles in the presence of fulvic acid, humic acid, or alginate: Effects of ionic composition. *Colloids Surf. A Physicochem. Eng. Asp.* **2011**, *379*, 21–26. [[CrossRef](#)]
30. Saleh, N.B.; Pfefferle, L.D.; Elimelech, M. Influence of biomacromolecules and humic acid on the aggregation kinetics of single-walled carbon nanotubes. *Environ. Sci. Technol.* **2010**, *44*, 2412–2418. [[CrossRef](#)]
31. Zieba, W.; Czarnecka, J.; Rusak, T.; Zieba, M.; Terzyk, A.P. Nitric-acid oxidized single-walled carbon nanohorns as a potential material for bio-applications—Toxicity and hemocompatibility studies. *Materials* **2021**, *14*, 1419. [[CrossRef](#)]
32. D’amora, M.; Camisasca, A.; Lettieri, S.; Giordani, S. Toxicity assessment of carbon nanomaterials in zebrafish during development. *Nanomaterials* **2017**, *7*, 414. [[CrossRef](#)]
33. Zhang, M.; Yudasaka, M.; Ajima, K.; Miyawaki, J.; Iijima, S. Light-assisted oxidation of single-wall carbon nanohorns for abundant creation of oxygenated groups that enable Chemical modifications with proteins to enhance biocompatibility. *ACS Nano* **2007**, *1*, 265–272. [[CrossRef](#)]
34. Yuge, R.; Manako, T.; Nakahara, K.; Yasui, M.; Iwasa, S.; Yoshitake, T. The production of an electrochemical capacitor electrode using holey single-wall carbon nanohorns with high specific surface area. *Carbon* **2012**, *50*, 5569–5573. [[CrossRef](#)]
35. Yamaguchi, A.; Kobayashi, M. Quantitative evaluation of shift of slipping plane and counterion binding to lysozyme by electrophoresis method. *Colloid Polym. Sci.* **2016**, *294*, 1019–1026. [[CrossRef](#)]
36. Jachimska, B.; Kozłowska, A.; Pajor-Świerzy, A. Protonation of lysozymes and its consequences for the adsorption onto a mica surface. *Langmuir* **2012**, *28*, 11502–11510. [[CrossRef](#)] [[PubMed](#)]
37. Kim, J.Y.; Ahn, S.H.; Kang, S.T.; Yoon, B.J. Electrophoretic mobility equation for protein with molecular shape and charge multipole effects. *J. Colloid Interface Sci.* **2006**, *299*, 486–492. [[CrossRef](#)]
38. Ohshima, H. *Theory of Colloid and Interfacial Electric Phenomena*, 1st ed.; Academic Press: Tokyo, Japan, 2006; Volume 12. Available online: [https://books.google.co.jp/books?id=X\\_\\_ekPRD-Z4C&printsec=frontcover&source=gbs\\_ge\\_summary\\_r&cad=0#v=onepage&q&f=false](https://books.google.co.jp/books?id=X__ekPRD-Z4C&printsec=frontcover&source=gbs_ge_summary_r&cad=0#v=onepage&q&f=false) (accessed on 8 February 2024).
39. Li, M.; Sugimoto, T.; Yamashita, Y.; Kobayashi, M. Aggregation and charging of natural allophane particles in the presence of oxyanions. *Colloids Surf. A Physicochem. Eng. Asp.* **2022**, *649*, 129413. [[CrossRef](#)]
40. Grolmund, D.; Elimelech, M.; Borkovec, M. Aggregation and Deposition Kinetics of Mobile Colloidal Particles in Natural Porous Media. *Colloids Surf. A Physicochem. Eng. Asp.* **2001**, *191*, 179–188. [[CrossRef](#)]
41. Wei, T.; Carignano, M.A.; Szeleifer, I. Molecular dynamics simulation of lysozyme adsorption/desorption on hydrophobic surfaces. *J. Phys. Chem. B* **2012**, *116*, 10189–10194. [[CrossRef](#)]

42. Israelachvili, J.; Pashley, R. Measurement of the Hydrophobic Interaction between Two Hydrophobic Surfaces in Aqueous Electrolyte Solutions. *J. Colloid Interface Sci.* **1984**, *98*, 500–514. [[CrossRef](#)]
43. Behrens, S.H.; Christl, D.I.; Emmerzael, R.; Schurtenberger, P.; Borkovec, M. Charging and Aggregation Properties of Carboxyl Latex Particles: Experiments versus DLVO Theory. *Langmuir* **2000**, *16*, 2566–2575. [[CrossRef](#)]
44. Molina-Bolívar, J.A.; Ortega-Vinuesa, J.L. How proteins stabilize colloidal particles by means of hydration forces. *Langmuir* **1999**, *15*, 2644–2653. [[CrossRef](#)]
45. Borkovec, M.; Papastavrou, G. Interactions between solid surfaces with adsorbed polyelectrolytes of opposite charge. *Curr. Opin. Colloid Interface Sci.* **2008**, *13*, 429–437. [[CrossRef](#)]
46. Trefalt, G.; Szilagyi, I.; Téllez, G.; Borkovec, M. Colloidal Stability in Asymmetric Electrolytes: Modifications of the Schulze-Hardy Rule. *Langmuir* **2017**, *33*, 1695–1704. [[CrossRef](#)] [[PubMed](#)]
47. Blomberg, E.; Claesson, P.M.; Froberg, J.C.; Tilton, R.D. Interaction between Adsorbed Layers of Lysozyme Studied with the Surface Force Technique. *Langmuir* **1994**, *10*, 2325–2334. [[CrossRef](#)]
48. Lotito, V.; Zambelli, T. Approaches to self-assembly of colloidal monolayers: A guide for nanotechnologists. *Adv. Colloid Interface Sci.* **2017**, *246*, 217–274. [[CrossRef](#)]

**Disclaimer/Publisher’s Note:** The statements, opinions and data contained in all publications are solely those of the individual author(s) and contributor(s) and not of MDPI and/or the editor(s). MDPI and/or the editor(s) disclaim responsibility for any injury to people or property resulting from any ideas, methods, instructions or products referred to in the content.